Inorganic Chemistry

pubs.acs.org/IC

Article

Mechanism of Hydroboration of CO_2 Using an Fe Catalyst: What Controls the Reactivity and Product Selectivity?

Asmita Sen, Mursaleem Ansari, and Gopalan Rajaraman*

Cite This: *Inorg. Chem.* 2023, 62, 3727−3737

Read Online

ACCESS | Metrics & More | Article Recommendations | Supporting Information

ABSTRACT: Using a combination of density functional theory (DFT) and ab initio complete active space self-consistent field (CASSCF) calculations, various elementary steps in the mechanism of the reductive hydroboration of CO_2 to two-electron-reduced boryl formate, four-electron-reduced bis(boryl)acetal, and six-electron-reduced methoxy borane by the $[Fe(H)_2(dmpe)_2]$ catalyst were established. The replacement of hydride by oxygen ligation after the boryl formate insertion step is the rate-determining step. Our work unveils, for the first time, (i) how a substrate steers product selectivity in this reaction and (ii) the importance of configurational mixing in contracting the kinetic barrier heights. Based on the reaction mechanism established, we have further focused on the effect of other metals, such as Mn and Co, on rate-determining steps and on catalyst regeneration.

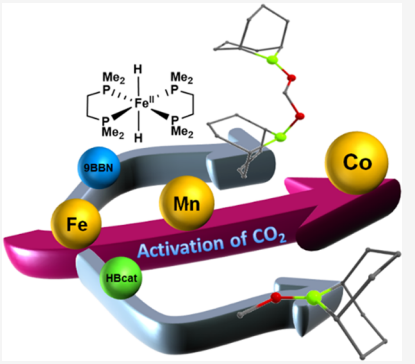

INTRODUCTION

Carbon dioxide is an abundant, nontoxic C1 source of carbon that has been proven to be economically beneficial in synthesizing fine and bulk chemicals in carbon capture technologies.[1−6] Despite the very high thermodynamic stability of the C═O bond, access to a full range of C-oxidation states has been made possible using metal-based molecular catalysts.[7−10] The most general way is the reduction of CO_2 in the presence of various reducing agents such as dihydrogen, silane, and boranes, which offers a milder reaction condition and facilitates the formation of CO, CH_2O, CH_3OH, and CH_4— a complete list of C1 compounds.[11−13] Several experimental studies have been performed on the conversion of CO_2 into value-added feedstocks, such as formic acid, formamides, salicylic acid, urea, etc., employing various electron-rich novel/base metal catalysts.[14,15] Examples include the hydrogenation reaction of CO_2 to formic acid and N-formylation products using PNP-pincer-supported Ru/Fe/Co(II) hydride catalysts achieving a turnover number of as high as 1 850 000.[16−19] Further advancements were made when Bontemps and co-workers, for the first time, reported the Ru-catalyzed CO_2 hydroboration reaction, forming the bis(boryl)acetal compound $[R_2BOCH_2OBR_2$, P$]$,[20] a four-electron-reduced product. Followed by this, earth-abundant hydride-dependent Fe(II) catalysts have also been employed in a one-pot, two-step strategy for the selective synthesis of bis(boryl)acetal, which can be used as a versatile and highly reactive source of methylene, which can be used in the formation of C−N/C−O/C−C/C═N/C═C bonds.[12] Experimentally, the catalytic hydroboration reaction of CO_2 was carried out in the presence of 9-borabicyclo[3.3.1]-nonane (9BBN) or catecholborane (HBCat) using 5 mol % of the $[Fe(H)_2(dmpe)_2]$ (**1**) (where dmpe is the 1,2-bis-(dimethylphosphino)ethane) catalyst under 1 atm of pressure. The product distribution is found to be completely substrate-dependent. While 9BBN is found to convert completely to four-electron-reduced bis(boryl)acetal (85%), catecholborane is selectively converted to six-electron-reduced methoxy borane.[12] Besides the substrate-dependent nature, the product distribution is, to some extent, also dependent on the nature of the metal ions, the presence of external additives such as Lewis acids and bases, etc. Substrate-dependent reduction products suggest that the substrate controls the mechanism of CO_2 activation, and an in-depth understanding of intricate mechanistic steps and the nature of rate-determining steps is needed for further development.[21,22] Second, the reported reaction is based on a rare Fe catalyst, but the literature precedent reveals that the mechanism and reactivity vary dramatically if alternate metal ions such as Ni/Co/Mn are used.[13,23−25] Moreover, understanding the mechanism of CO_2 activation by first-row transition elements is challenging due to the involvement of different spin states, various spin configurations, and intricate mechanistic steps.

Apart from Fe, other transition metals like Co and Mn are also explored and proven to be good catalysts for small

Received: August 5, 2022
Published: February 20, 2023

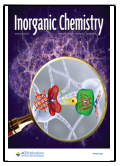

https://doi.org/10.1021/acs.inorgchem.2c02812
Inorg. Chem. 2023, 62, 3727−3737

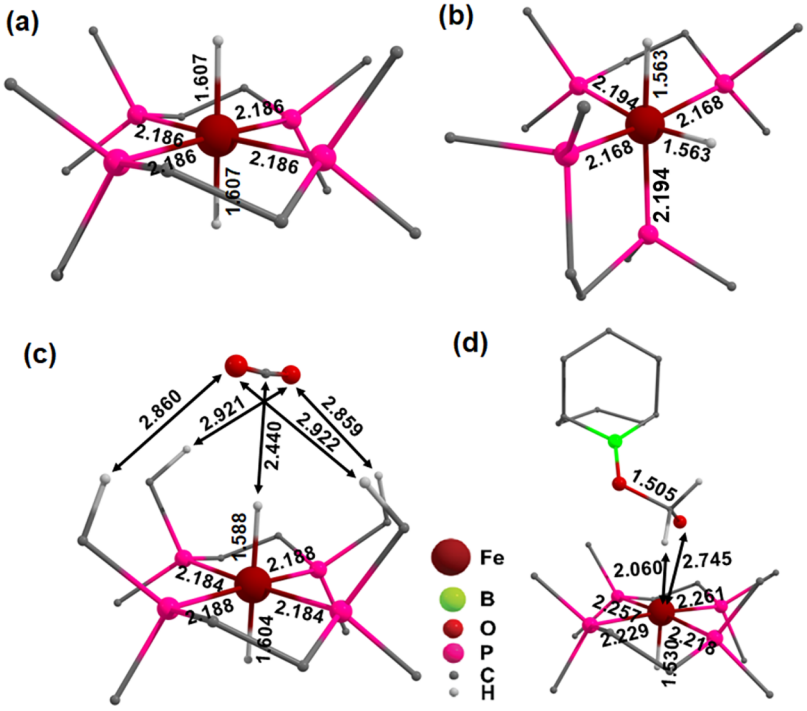

Figure 1. DFT-optimized structures of (a) R_t, (b) R_c, (c) RC_t, and (d) rate-determining $TS6_t$ showing important bonding parameters. Fe, P, O, B, C, and H atoms are shown in brown, pink, red, green, gray, and white colors, respectively.

molecule activation like CO_2.[9,18,26−29] Complexes such as the $^{iPr}PN^HP$-supported Co(II) chloride complex [($^{iPr}PN^HP$)-$CoCl_2$] reported by Beller and Milstein are found to be promising during the N-formylation of dimethyl and diethylamine with good turnover numbers. This inspired us to examine the effect of these metals in the hydroboration reaction of CO_2. To untangle these issues, here, we have employed DFT [M06-L/def2-TZVPP//UM06L/LanL2DZ-(Fe)[6-31G(d)(rest)]] and ab initio CASSCF calculations to shed light on the mechanism of the reduction of CO_2 to bis(boryl)acetal catalyzed by **1** and extended our study to other in silico models where instead of Fe, Mn(2) and Co(3) ions are utilized.[30,31]

COMPUTATIONAL DETAILS

Geometries of all stationary points were optimized without restrictions by the density functional theory calculations using the Gaussian 16 (Revision C.01) suit.[32] A meta-GGA (GGA = generalized gradient approximation) M06-L density functional[33] is employed in conjunction with a double-ξ quality LanL2DZ basis set with Los Alamos effective core potential[34] for metal (Fe) and the 6-31G(d) basis set for the rest of the atoms such as H, B, C, O, and P. The functional is chosen based on the earlier literature and benchmarking available on similar systems and the ability of the M06-L functional to account for noncovalent interactions. For instance, Truhlar and co-workers have shown that the meta-GGA M06-L density functional can successfully reproduce the ground state of most of the Fe(II)/Fe(III)/Fe(IV) species under investigation.[35] The Ye and Neese group have investigated the CO_2 hydrogenation reactions catalyzed by $[M(H)(\eta^2\text{-}H_2)(PP_3^{Ph})]^{n+}$ (M = Fe(II), Ru(II), and Co(III); PP_3^{Ph} = tris(2-(diphenylphosphino)phenyl)phosphine) complexes. The mechanistic steps established using this protocol are found to be in agreement with the experimental data, offering confidence in the chosen methodology.[36] The harmonic vibrational frequency calculations have been performed to characterize the nature of all stationary points and also to compute the zero-point energy corrections on them. All global minima are characterized by all positive frequencies, while the transition state is characterized by a single imaginary frequency. Intrinsic reaction coordinate (IRC) calculations were carried out at the same level to ensure that the transition states connect the minima on either side of the saddle point. The refinement of the energies was performed by single-point calculations on the optimized structures in the same level of theory using an all-electron def2-TZVPP basis set.[37] The solvent effect on the refined energies has been counted employing the SMD solvation model[38] using tetrahydrofuran (THF) as the solvent. The final energies considered in the present study are the zero-point energy-corrected solvation energies at the higher level. The deformation energy (ΔE_{def}) analysis has been performed to obtain the destabilizing steric energy associated with the transition states. The transition states were divided into two fragments, A (catalyst part) and B (substrate part). The solvent-phase single-point calculations, as well as frequency calculations, have been performed on them. Then, the summation of these two energies is subtracted from the summation of energies of the free catalyst and the substrate ($E_{solvation}$ + ZPC).

Therefore,

$$\Delta E_{def} = TS(A + B)(E_{solvation} + ZPC) - A(E_{solvation} + ZPC) - B(E_{solvation} + ZPC)$$

All ab initio single-point calculations were carried out on the DFT-optimized geometries of the intermediates and the transition states using the ORCA 4.2.1 program.[39] The Douglas−Kroll−Hess (DKH) Hamiltonian[40] has been used to account for the scaler relativistic effects. The DKH-

https://doi.org/10.1021/acs.inorgchem.2c02812
Inorg. Chem. 2023, 62, 3727−3737

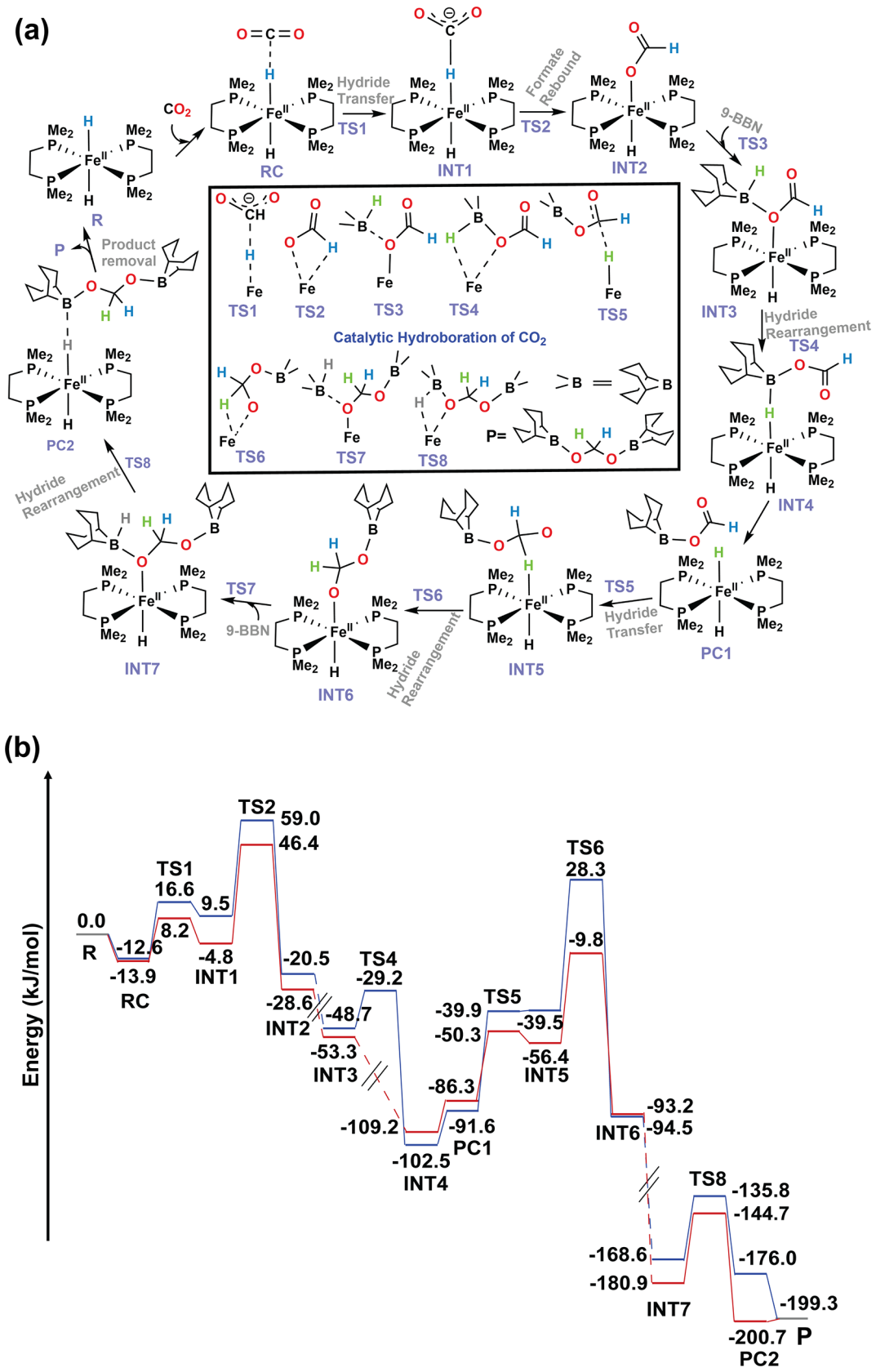

Figure 2. (a) Schematic representation of various stationary points involved during the $Fe^{II}(H)_2(dmpe)_2$-catalyzed reductive hydroboration of CO_2 to bis-boraylacetal and (b) DFT-computed potential energy diagram (kJ/mol) of the $Fe^{II}(H)_2(dmpe)_2$-catalyzed reductive hydroboration of CO_2 to bis-boraylacetal using 9BBN. Red and blue lines are for *trans*- and *cis*-catalysts, respectively.

https://doi.org/10.1021/acs.inorgchem.2c02812
Inorg. Chem. 2023, 62, 3727−3737

contracted version of the basis sets, such as DKH-def2-TZVP for Fe, DKH-def2-TZVP(-f) for directly coordinated atoms (P, O, H) to the metal, and DKH-def2-SVP for the rest of the atoms, which are not directly connected to the metal, has been used. The next step was the orbital optimization step using state-averaged complete active space self-consistent field (SA-CASSCF)[41] calculations, which were also performed using the same basis set. The Fe center remains in a +II oxidation state throughout the pathway. Therefore, CAS(6,5) calculations have been performed in all transition states involved during the formation of bis(boryl)acetal, including six metal d-electrons distributed in 5 metal d-orbitals. For these CAS(6,5) calculations, 5 quintet, 45 triplet, and 50 singlet roots have been considered. We have extended the reference space, including the hydride and boron orbitals, and performed additional calculations to check the validity of the methodology employed.

All stationary points were denoted as $^{(2S+1)}Y_{c/t}$. Here, Y is RC for reactant complex, INT for intermediates, and TS for transition states, and c/t denotes either a *cis*-isomer or a *trans*-isomer form of the catalyst. The overall spin multiplicity is stated as superscript in the extreme left to the general description as (2S + 1). The stationary points denoted by the cat subscript belong to the catecholborane substrate.

RESULTS

Reactivity of 1 towards the Four- and Six-Electron Reduction of CO_2. To begin with, we have looked at various spin states of **1**, and our DFT calculations (Tables S1 and S2) yield an $S = 0$ low spin state as the ground state for both the *cis*-isomer and *trans*-isomer of **1** ($\mathbf{1}_c$ and $\mathbf{1}_t$) with the $S = 2$ high spin and $S = 1$ intermediate spin states found to lie above 145.0 kJ/mol. All other transition states in the potential energy surface are lower than this energy (vide infra), which eliminates the possibility of the involvement of other paramagnetic spin states in the reaction mechanism. However, configurational mixing among various $S = 0$ states cannot be ruled out. A very large energy gap observed for these spin states is due to the very strong ligand field present at the metal center and the nature of the *d*-electronic configuration. The geometry of $\mathbf{1}_t$ is highly symmetric, with all Fe−P (2.186 Å) and Fe−H bonds (1.607 Å) being equal (Figure 1a). In $\mathbf{1}_c$, the symmetry is lifted with different Fe−P distances (Figure 1b), inaxial and equatorial positions (2.168 Å vs 2.194 Å). Also, the Fe−H distances in $\mathbf{1}_c$ are shorter than $\mathbf{1}_t$ (1.563 Å). Our calculations reveal that the longer Fe−H bond length in $\mathbf{1}_t$ is due to the presence of the strong trans effect of the hydride ligand. *Trans*-isomers have a longer Fe−H bond, resulting in a significant increase in the hydricity of each Fe−H moiety, which, in turn, makes them more likely to deliver H^- to polar-containing double bonds such as CO_2 compared to the *cis*-isomer. As depicted in Figure 2, both the schematic diagram and the reaction energetics of the hydroboration of CO_2 using an iron-based catalyst provide a deeper understanding of the reaction mechanism. Here, all optimized geometries of the stationary points are depicted in Figures S1−S5. The reductive hydrogenation initiates via the partial activation of CO_2 at reactant complex species (RC_t/RC_c: −13.9/−12.6 kJ/mol) via (methyl)C−H···O(CO) (2.860 Å, 2.859 Å, 2.921 Å, and 2.922 Å and 2.5 Å, 2.679 Å, 2.686 Å, and 2.832 Å, respectively, in RC_t and RC_c) and (Fe)H···C(O_2) (2.440 and 2.497 Å) noncovalent interactions (Figure 1c). The anchoring of the CO_2 molecule in the vicinity of the metal was found to reduce the corresponding Fe−H bond distances, 1.588; 1.554 Å and 1.554; 1.559 Å compared to the free catalyst in the *trans*- and *cis*-isomers, respectively. In the next step, hydride transfer to the electron-deficient C_{CO_2} takes place, forming a hydride-bound intermediate, INT1, which is endothermic by 9.1 and 22.1 kJ/mol from RC for the *trans*- and *cis*-isomers, respectively. The intrinsic energy barrier for this hydride transfer is minimal and is estimated to be 8.2 kJ/mol ($TS1_c$: 16.6 kJ/mol). In TS1, the iron-bound hydride attacks the electron-deficient C-atom from a distance of 1.670 Å (1.583 Å in *cis*-isomer), which in the next step (INT1) forms a complete (Fe)H−C(O_2) bond ($INT1_t/INT1_c$: 1.232 and 1.249 Å) with an elongation in the Fe−H(CO_2) ($INT1_t/INT1_c$: 1.662 and 1.683 Å) bond. All bonding parameters indicate that in INT1, the formate is loosely bound to the metal center through the hydride ligand. This subsequently undergoes a formate rebound transition state (TS2), where the weak Fe−H bond is broken, and a new Fe−O bond is formed, resulting in oxygen-bound formate Fe−O(CHO) species (INT2). Due to the formation of a stable Fe−O bond (2.076 Å) in INT2, in place of a weak Fe−H bond in INT1, the conversion is highly exothermic ($INT2_t/INT2_c$: −28.6/−20.5 kJ/mol).

The energy barrier for the formate rebound is found to be 51.2 and 49.5 kJ/mol for $TS2_t$ and $TS2_c$, respectively. The next step is the addition of 9BBN to the Fe−O bond in INT2 via TS3, and this is found to be a barrierless process. We have performed a potential energy surface scan along the Fe−O···B(9BBN) bond and found a decrease in energy as the O···B bond length decreases. This results in the formation of an Fe−O(9BBN)(CHO) species (INT3) whose formation is exothermic (−53.3 and −48.7 kJ/mol for the *trans*- and *cis*-isomers, respectively) from INT2. A strong charge polarization in the (Fe)O−B(9BBN) bond (−0.619 vs 0.505) in INT3 is a driving force for its barrierless formation. After (Fe)O−B(9BBN) bond formation, the Fe−O and O−C(HO) bonds get elongated ($INT3_t/INT3_c$: 2.341/1.315 Å and 2.182/1.318 Å) compared to INT2, preparing the system for further rearrangement (TS4) where the Fe−O bond will cleave with the simultaneous formation of the Fe−H(9BBN) bond. This step is barrierless for the *trans*-isomer and has only a 19.5 kJ/mol energy barrier for *cis*-ones from INT3. Similar to TS3, we have performed a potential energy surface scan along the Fe−H and Fe−O distances and found a constant decrease in energy as the Fe−H bond started breaking and the Fe−O bond started to form. The intrinsic energy barriers for TS4 are in accordance with the Fe−O bond length in INT3; a longer Fe−O bond in the *trans*-isomer results in a smooth barrierless transition. This results in INT4, where the 9BBN−O(CHO) moiety is found to be attached to the Fe center through a weak (Fe)H···B(9BBN) bond, and this intermediate is found to lie at −102.5 kJ/mol ($INT4_c$: −109.2 kJ/mol) downhill from the free catalyst. This moiety cleaves from the metal, regenerating the free catalyst and 9BBN(OCHO) species—the first $2e^-$-reduced product from the CO_2 reduction (PC1). The catalyst regeneration, along with the formoxy (9BBN(OCHO)) production, is highly exothermic in nature for both *trans*- and *cis*-catalysts by −86.3 and −91.6 kJ/mol, respectively.

The first catalytic cycle completes at this step, and the freshly formed 9BBN(OCHO) species again reacts with the regenerated catalyst in the next step. Once again, the electron-rich hydride center attacks the electron-deficient carbonyl center of 9BBN(O═CHO), which results in the formation of

https://doi.org/10.1021/acs.inorgchem.2c02812
Inorg. Chem. 2023, 62, 3727−3737

INT6. This second hydride transfer is found to be associated with an energy barrier of 58.9 kJ/mol from PC1. The energy barrier for the second hydride transfer is found to be very high compared to the first hydride transfer step (TS1 vs TS5; 8.2 kJ/mol vs 58.9 kJ/mol), and this is attributed to the lower electrophilic nature of the carbonyl carbon of 9BBN(O═CHO). This is evident from the computed NPA charges on the carbonyl carbon atom, which are found to be reduced drastically in PC1 viz-a-viz RC (0.982 vs 0.594). In the next step, INT6 undergoes a rebound process where the newly formed Fe−H bond breaks, and at the same time, Fe−O(CHO) is formed via TS6 (Figure 1d), with an intrinsic barrier of 46.6 kJ/mol ($TS6_c$: 67.8 kJ/mol). Although the energy barrier of this rearrangement is lower than the intermediate (INT6), the energy barrier from the lowest energy intermediate (INT4) is steep (99.4 kJ/mol). Therefore, this rearrangement step is considered the rate-determining transition state (TDTS). In INT6, an Fe−O (2.070 Å) bond is formed, and at this step, another 9BBN molecule is attached to the Fe-bound oxygen center in a barrierless manner, forming INT7. The attachment of another borane molecule is found to be significantly exothermic ($INT7_c$ and $INT7_t$: −168.6 and −180.9 kJ/mol). The next step is the catalyst regeneration step, where INT7 undergoes a rebound mechanism transition state (TS8), cleaving the strongly attached Fe−O bond and forming a weak Fe−H(9BBNCH$_2$9BBN) bond. This product (PC2) dissociates to produce bis(boryl)acetal and the regenerated catalyst. Although this dissociation is slightly endothermic (1.4 kJ/mol), the overall energy gain during this pathway is very high (199.3 kJ/mol, P). The energetic gain in the catalyst regeneration is carried forward to the next cycle, facilitating the reaction and enhancing the reaction rate as well as turnover number. The energetics associated with $\mathbf{1}_c$ and $\mathbf{1}_t$ reveal that the energy barriers between INT4 (rate-determining intermediate, TDI) and the rate-determining transition state (TS6) [ΔE(TDI−TDTS)] are estimated to be 137.5 and 92.7 kJ/mol, respectively. Although both isomers are found to react via an exothermic process, the energy requirement in the rate-limiting step for the *cis*-isomer is 44.8 kJ/mol higher than that for the *trans*-isomer, indicating the greater reactivity of the latter. As the *trans*-isomer is more reactive, the possibility of interconversion at the resting state of the catalyst from the *trans*-isomer to the *cis*-isomer is explored by performing a relaxed potential energy surface scan (Figure S6) along the H−Fe−H angle from 180° (*trans*-isomer) to 90° (*cis*-isomer). This yielded a qualitative barrier height of ∼120 kJ/mol at a H−Fe−H angle of 120°, suggesting a steep energy penalty for interconversion as a free catalyst. However, once the reaction is triggered, abstraction of one of the hydrides from the *cis*-isomer could facilitate the interconversion as the ligand can rearrange from distorted trigonal pyramidal to square planar upon removal of one of the hydride ligands as formate.

Substrate-Dependent Product Distribution. Experimentally, it was found that the two different boranes lead to the formation of two different products; while 9BBN results in the formation of four-electron-reduced bis(boryl)acetal, catecholborane leads to a six-electron-reduced product, methoxy borane.[12] In this section, we have extended our mechanistic studies to understand substrate dependency in product distribution. After the formation of INT6, another possibility is the removal of the formaldehyde molecule (Scheme 1). The newly forming HCHO can undergo a hydride transfer process with catalyst **1**, which leads to the formation of methoxy borane, as shown in Scheme 2. With 9BBN, the energy barrier for the removal of HCHO ($TS7_a$) is estimated to be high, 90.7 kJ/mol (Figures 3 and S7a), forming $INT7_a$ (−5.1 kJ/mol). The very high energy barrier for the removal of HCHO eliminates the possibility of the formation of methoxy borane in the case of 9BBN. Therefore, the product distribution is mainly decided at the stage of INT6, where the entry of another borane leads to the formation of INT7, facilitating bis(boryl)acetal production. Therefore, it is expected that if the energy penalty for conversion to INT7 via TS7 is high and at the same time, if the HCHO removal step is not energetically demanding, it leads to the formation of methoxy borane. The HCHO molecule, after removal, can react with another catalyst ($\mathbf{1}_t$), forming $INT1_b$ via $TS1_b$ (3.9 kJ/mol). $INT1_b$ undergoes a rearrangement, forming the Fe−OCH_3 intermediate ($INT2_b$) via $TS2_b$ (54.4 kJ/mol), which in the next step attaches to another 9BBN molecule, forming $INT3_b$. $INT3_b$ then undergoes another rearrangement reaction, forming $\mathbf{1}_t$ and methoxy borane (PC4). From the overall energetics, it is found that none of the steps involved in the mechanism is higher in energy; all of them lie below 54.4 kJ/mol (Figure 3). Therefore, it does not affect the rate or product selectivity; it is the formaldehyde removal step that decides the product distribution depending on various boranes.

Scheme 1. Schematic Representation of the Removal of HCHO during Hydroboration of CO_2 in the Presence of 9BBN

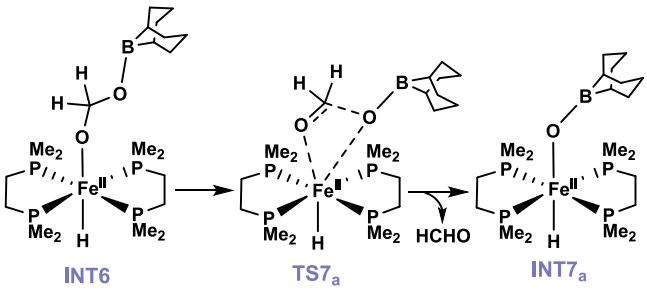

To further understand the different product formations with different boranes (here, 9BBN and HBCat), we have computed the energetics for the formation of bis(boryl)acetal versus methoxy borane with the substrate HBCat. The geometries of all stationary points corresponding to the substrate HBCat are shown in Figures S8 and S9. Figure 4 shows that the introduction of the first HBCat molecule to the catalyst ($\mathbf{1}_t$) is exothermic ($INT3_{cat}$: −44.8 kJ/mol). In the next step, the replacement of the Fe−O(HBCat)(CHO) bond by an Fe−H(HBCat) bond takes place via a rearrangement transition state $TS4_{cat}$ (13.5 kJ/mol from $INT3_{cat}$), which is found to be exothermic by −50.5 kJ/mol ($INT4_{cat}$). The formation of the first 2e$^-$-reduced product HBCat(OCHO) species is slightly endothermic ($PC1_{cat}$: 43.3 kJ/mol). At this stage, the hydride attacks the HBCat(OCHO) molecule, forming $INT5_{cat}$ via $TS5_{cat}$. This step is endothermic by 19.3 kJ/mol from $PC1_{cat}$, and the energy required for this step is 27.8 kJ/mol. The $INT5_{cat}$ then undergoes a rearrangement, forming $INT6_{cat}$ (−70.8 kJ/mol) via $TS6_{cat}$ with an energy barrier of 28.9 kJ/mol. At this stage, either it can remove a HCHO molecule via $TS7a_{cat}$, forming $INT7a_{cat}$ and leading to the formation of methoxy borane, or a second HBCat molecule can approach and form $INT7_{cat}$ via $TS7_{cat}$. $INT7_{cat}$ will lead to

https://doi.org/10.1021/acs.inorgchem.2c02812
Inorg. Chem. 2023, 62, 3727−3737

Scheme 2. Schematic Representation of the Formation of Methoxy Borane (BR_2OCH_3) during the Hydroboration of CO_2 in the Presence of 9BBN

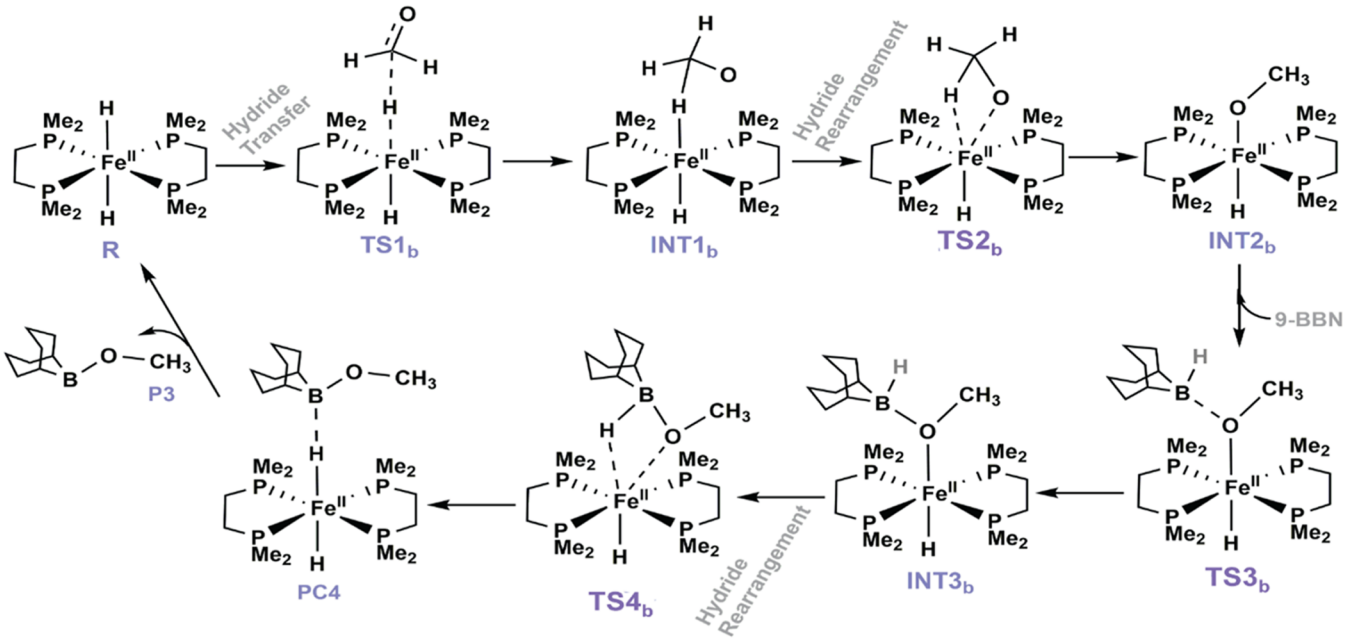

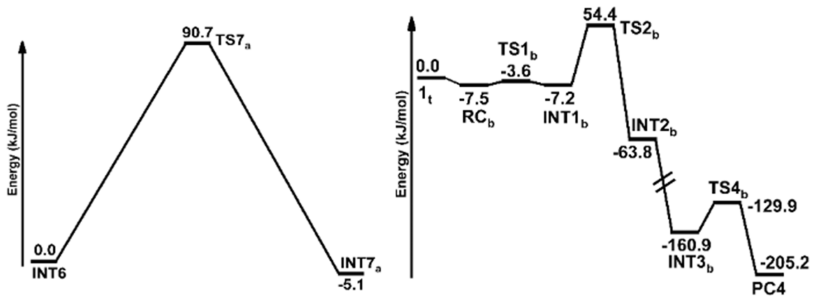

Figure 3. DFT-computed potential energy diagram (kJ/mol) of the removal of HCHO and its reaction with $\mathbf{1}_t$ forming methoxy borane.

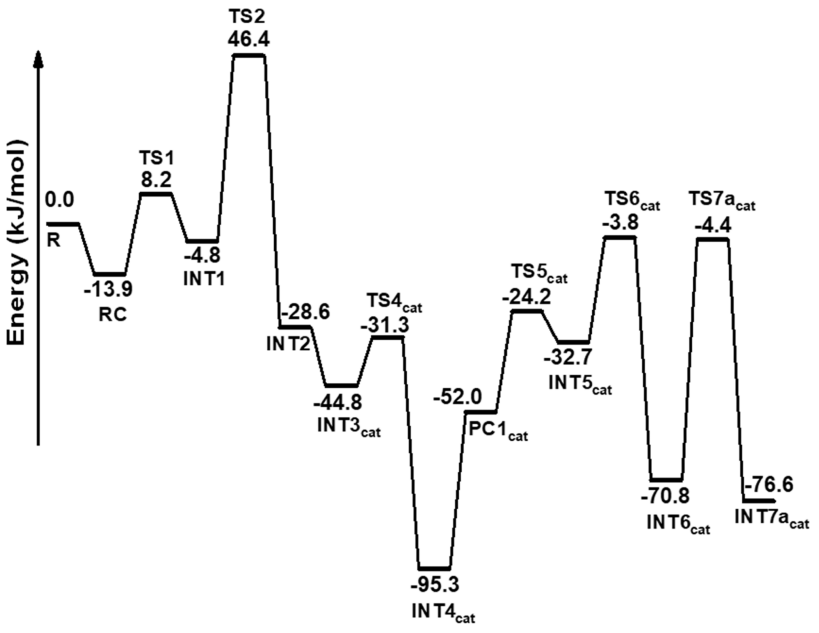

Figure 4. DFT-computed potential energy diagram (kJ/mol) of the *trans*-$[Fe^{II}(H)_2(dmpe)_2]$-catalyzed reductive hydroboration of CO_2 to methoxy borane using HBCat substrate.

https://doi.org/10.1021/acs.inorgchem.2c02812
Inorg. Chem. 2023, 62, 3727−3737

the formation of bis-boraylacetal and a free catalyst. The energy required for HCHO removal is lower by ∼24 kJ/mol, suggesting that this step is energetically favored. To estimate the energy requirement for the latter step (addition of the second HBCat molecule), a relaxed potential energy surface scan (Figure S10) along the (Fe)O−BR_2 bond is performed, which reveals that the overall energy of the system increases more steeply in the case of BR_2 = HBCat compared to BR_2 = 9BBN (∼85 kJ/mol vs 65 kJ/mol). Therefore, attaching a 9BBN molecule is comparatively more facile than attaching a HBCat molecule at INT6 at any point.

Role of Other Metals in Catalytic Efficiency. In this section, we intend to check the scope for other 1st-row transition metal ions such as Mn (**2**) and Co (**3**) as a catalyst.[42] For catalysts **2** and **3** as well, the high and intermediate spin states were also found to lie significantly higher in energy (>56 kJ/mol). Therefore, these spin states are not considered in the further reaction. The M−H bond is elongated in the Mn catalyst (1.673Å) and shortened in the Co catalyst (1.586 Å, Figure S7) compared to the Fe one. As we are looking for a better catalyst in terms of turnovers, we have focused only on the rate-determining step and the catalyst regeneration steps for **2** and **3**. Energetics reveals that the energy barriers between INT4 and rate-determining TS6 [Δ*E*(TDI−TDTS)] are estimated to be 73.9 kJ/mol and 42.2 kJ/mol, respectively, for Mn and Co, respectively (Figure 5).

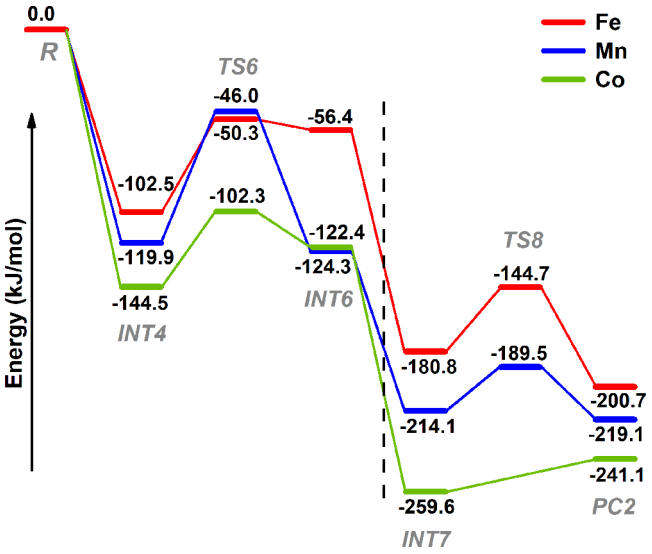

Figure 5. Comparative DFT-computed potential energy diagram (kJ/mol) of **1**−**3** showing the rate-determining step (R to INT6 before the black vertical line) and catalyst regeneration steps (INT7 to PC2 after the black vertical line).

Similarly, the energy requirement for the catalyst regeneration is found to be 36.1 kJ/mol in the case of the Fe catalyst, while it is 2467 kJ/mol for the Mn catalyst. In the catalyst regeneration process, an Fe−O(9BBN)(CH_2O9BBN) species is involved in a rearrangement process where the Fe−O bond is cleaved, and a new Fe−H(CH_2) bond is formed. In catalyst **3**, the Co−O bond is not fully formed in INT7, but the 9BBN−CH_2−O−9BBN moiety is loosely bound to the metal center. Therefore, it is anticipated that in **3**, no significant barrier is present in the catalyst regeneration process. As soon as a second 9BBN molecule gets attached to INT6 [Co−OCH_2(9BBN)], the Co−O bond becomes longer (Figure S11). Therefore, for **3**, this step itself is the catalyst regeneration step. These suggest that although the energy barrier for the rate-determining step is comparable for all these three catalysts, the catalyst regeneration steps are less energy demanding for catalysts **2** and **3** and are likely to be better catalysts than **1** if made.

Factors Controlling the Barrier Height. The participation of the open-shell configuration of the same spin multiplicity in controlling the reactivity of high-valent Mn^{IV}=O species is well known,[43−45] although the role of these paramagnetic spin states in the low-valent systems was not explored. This motivated us to look at the role of electronic flexibility and various spin configurations in influencing the reaction barrier. Apart from the electronic factor, we have also considered the steric requirements in the transition states. Figure 6 shows the dependency of barrier height on the

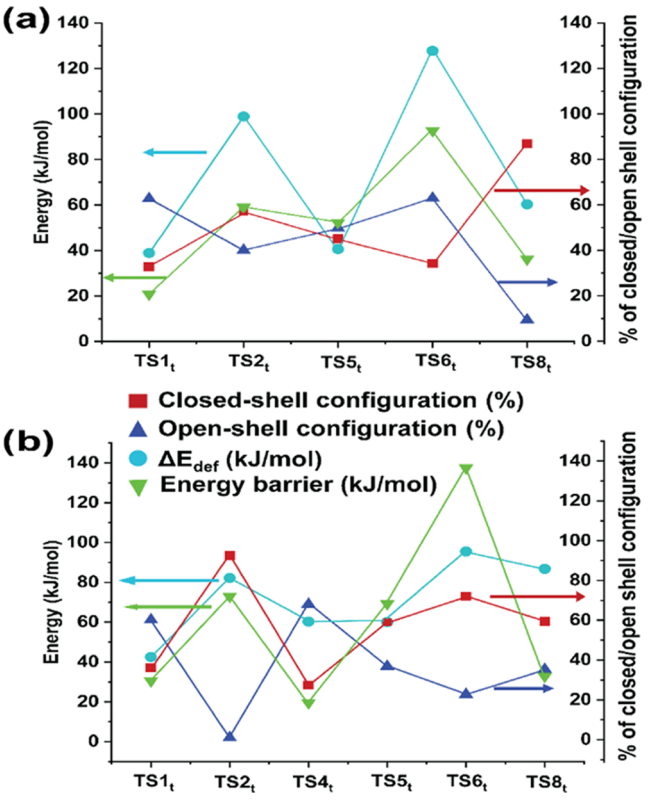

Figure 6. Graphical representation of the dependence of the energy barrier of (a) *trans*- and (b) *cis*-Fe(II) species on various factors such as electronic flexibility and steric requirement. Green symbols correspond to the energy barrier for transition states. Cyan symbols are for the estimated deformation energy of transition states. Red and blue symbols correspond to % of closed- and open-shell configurations, respectively. The *Y*-axis on the left side corresponds to energy (kJ/mol), while on the right side, it is % values.

aforementioned factors. Herein, we attempted to draw a correlation between the energy barrier and various factors that control the barrier height.

We have explored various *S* = 0 spin configurations apart from the closed-shell $(d_{xy})^2(d_{yz})^2(d_{xz})^2$ configuration for the Fe(II) ion. This includes other open-shell singlet states such as $(d_{xy})^1(d_{yz})^2(d_{xz})^2(d_{x^2-y^2})^1$ or $(d_{xy})^2(d_{yz})^2(d_{xz})^1(d_{z^2})^1$. Our CAS-(6,5) calculations on the transition state structures reveal significant mixing of the open-shell singlet configuration (blue symbols) with the closed-shell one (red symbols) during the

https://doi.org/10.1021/acs.inorgchem.2c02812
Inorg. Chem. 2023, 62, 3727−3737

CO_2 hydroboration reaction and this is similar to earlier observations on different Fe(II) catalysts.[46] The computed data clearly indicate that higher electronic flexibility, i.e., stronger mixing of the closed-shell singlet state with the open-shell singlet configuration, results in a lower energy barrier. For instance, $TS1_{t/c}$ has a larger contribution from the $(d_{xy})^1(d_{yz})^2(d_{xz})^2(d_{x^2-y^2})^1$ configuration (62.8/61.2%) compared to a smaller contribution from the closed-shell singlet state (32.8/37.0%; Table S3). Because of this, the barrier height for $TS1_{t/c}$ is very small. In contrast, the energy barrier in $TS2_{t/c}$ is quite high, which is found to be directly correlated to a dominant closed-shell singlet with small mixing of the open-shell configuration (57.0/93.4% and 40.1/2.0%, respectively). The lowering of the energy barrier with higher mixing can be rationalized, as larger mixing of open-shell configuration promotes the d-electron to the antibonding $d_{x^2-y^2}/d_{z^2}$ orbital, which facilitates greater metal−ligand repulsion, leading to longer Fe···H/O distances and a facile Fe···H/O cleavage at the transition state. Thus, the d-electronic flexibility is critical to the estimation of barrier heights. We have extended the CAS reference space, and the results are found to be similar. For instance, in TS1, we have included the hydride orbitals in the CAS reference space and performed CAS(8,6) calculations, revealing that the contribution from the open-shell configuration remains similar (59.4%). Further, in TS6, after the inclusion of H and B orbitals, the contribution from the open shell remains similar, reaffirming our point on the role of such configurational mixing in controlling the energy barriers.

In the rate-determining $TS6_t$, although a higher contribution from the open-shell configuration is observed (63%), the energy barrier is found to be very high (99.4 kJ/mol). This is attributed to a very high steric requirement (127.8 kJ/mol, see cyan color lines), and such unfavorable steric more than compensates for the energetic gain due to the open-shell configuration, leading to a larger barrier. Thus, while the open-shell configurational mixing certainly helps reduce the barrier height, if other factors override this contribution, the reactivity will likely to be sluggish. As steric contributions to the transition states can be controlled by ligand design, and it is a well-established concept in this chemistry, this offers ample room to improve the catalytic turnover based on configurational mixing.

DISCUSSION

Various experimental and computational studies have been performed on the area of CO_2 activation, and rate-determining steps have been identified. Based on the nature of the rate-determining steps, various modifications have been implemented in terms of the metal center, ligand architecture, and metal oxidation states to fine-tune the reaction barrier. It is observed that during the reduction of CO_2 to formic acid, while in some studies, the first hydride transfer step has been identified as the rate-limiting, some are associated with the heterogeneous H_2 cleaving. For instance, the CO_2 activation reaction by PNP-pincer (where PNP represents 2,6-bis-(dialkylphosphinomethyl)-pyridine-based $Fe^{II}/Co^{III}/Ru^{III}$ catalysts, namely, $[(PNP)Ir^{III}(H)_3]$, $[(PNP)Co^{III}(H)_3]$, and $[(PNP)Fe^{II}(H)_2(CO)]$) results in an H_2 splitting step[47,48] as the rate-determining step, while the hydride transfer step is identified as rate-limiting with the $h[(\eta^5\text{-}C_5Me_5)Ir^{III}(bpy)(H)]^+$ catalyst.[49] Neese and co-workers have shown that the rate-defining step for CO_2 hydrogenation in $[M(H)(\eta^2\text{-}H_2)(PP_3^{Ph})]^{n+}$ species ($M = Fe^{II}/Co^{III}$) is decided by the hydricity of the metal−hydride intermediate forming via H−H splitting.[36,47] While H−H splitting is the rate-determining step for the Fe^{II} catalyst, it is the hydride transfer for the Co^{III} one. Therefore, careful identification of the correct rate-limiting step in similar reactions is crucial for the generation of future catalysts.

While CO_2 hydrogenation is a well-established process and various mechanistic steps have been identified, mechanistic exploration of the hydroboration of CO_2 using 1st-row transition metal catalysts is limited. Experimentally, Bontemps and Hazari's group have shown how Fe^{II} and Ni^{I} catalysts can be useful for the selective reduction of CO_2 either in two-, four-, or six-electron reduction levels depending on the nature of the catalyst, substrate, and reaction conditions.[25] Although the experimental studies have explained various aspects in terms of product distribution and selectivity, studies at the molecular level, which involve the estimation of different transition states, are pivotal. Using density functional theory calculations, we have successfully captured various intermediates such as two-electron-reduced boryl formate, four-electrons-reduced bis(boryl)acetal, and finally, six-electron-reduced methoxy borane, and these are in line with the experimental observations.[25] In the present case, we have found that the hydroboration of CO_2 to four-electron-reduced bis(boryl)acetal follows six main steps: (i) first, hydride transfer to CO_2, (ii) formate rebound, followed by the first borane addition, (iii) removal of the two-electron-reduced product and 1st regeneration of the free catalyst, (iv) the second hydride transfer to the newly formed two-electron-reduced product, (v) second borane addition, and finally, (vi) the formation of four-electron-reduced bis(boryl)acetal via hydride rearrangement. Among them, the formation of the Fe−O bond by replacing the Fe−H bond (TS6, after the boryl formate formation) is found to be the rate-limiting step.

Experimentally, the selectivity for the two-electron-reduced boryl formate increases with the increase of CO_2 pressure, which is consistent with the proposed mechanistic insights. The energy barrier for the second hydride attack to the boryl formate (TS5) is relatively larger than that for the first hydride attack. Therefore, in high CO_2 concentrations, the freshly generated catalyst in PC1 will prefer to react with another CO_2 molecule forming boryl formate selectively. In a low CO_2 concentration, the insertion of boryl formate is expected to be facilitated, and the reaction leads to the formation of bisborylacetal as a product.

While the product selectivity with respect to different substrates is noted in the experiments, the step responsible for the product selectivity is not elucidated. The product formation is found to be strongly dependent on the nature of the substrate, with 9BBN yielding four-electron-reduced bis(boryl)acetal (85%) as a major product and HBCat converting to the six-electron-reduced methoxy borane.[12] Our calculations suggest that the more facile the attachment of the second borane to the $Fe{-}O(CH_2)O{-}BR_2$ species (INT6), the easier the bis(boryl)acetal formation. At the same time, the $Fe{-}O(CH_2)O{-}BR_2$ species (INT6) can remove HCHO, which in the next step, leads to the formation of methoxy borane. Therefore, the energy required for the removal of HCHO will decide the formation of methoxy borane. A lower kinetic energy barrier for this step facilitates methoxy borane formation. Therefore, the fate of product formation is extremely dependent on the delicate balance between the energy requirement of the two transition states,

https://doi.org/10.1021/acs.inorgchem.2c02812
Inorg. Chem. 2023, 62, 3727−3737

TS7 and TS7a. A careful analysis of Figure 7 reveals that the intermediates involved in the pathway of 9BBN are more

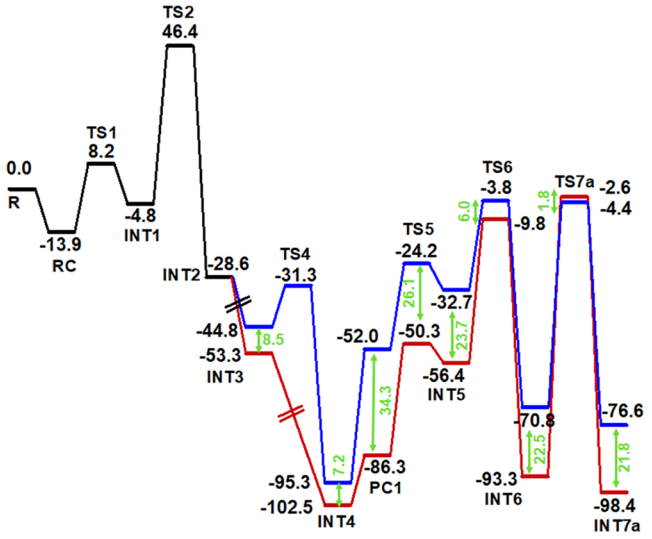

Figure 7. Comparative DFT-computed potential energy diagram (kJ/mol) of the *trans*-[$Fe^{II}(H)_2(dmpe)_2$]-catalyzed reductive hydroboration of CO_2 to methoxy borane using 9BBN (blue) and HBCat (red) substrate. The energy gap (kJ/mol) in each step is shown in green.

stable than the same with HBCat. The first hydride rearrangement (TS4) and the next hydride attack transition state (TS5) are destabilized in the case of HBCat compared to 9BBN, though the other transition states are lying closely (differ by ∼6 kJ/mol). However, these two transition states are not rate-determining and, therefore, cannot affect the rate of the reaction. Although the barrier for the HCHO removal transition state (TS7a) differs only 2.0 kJ/mol for both substrates, INT6 is significantly stabilized (22.5 kJ/mol) for 9BBN, increasing the energy penalty (24.3 kJ/mol) for the formaldehyde removal for 9BBN. Therefore, when 9BBN is used as a substrate, the bis-boraylacetal formation will be favored. While this step is comparatively facile for HBCat (66.4 kJ/mol), the introduction of a second HBCat molecule requires higher energy (>20 kJ/mol), leading to the formation of methoxy borane as a major product. This results in product selectivity depending on the nature of the substrate employed.[50−52]

The higher stability and reactivity of the *trans*-isomer than those of the *cis*-isomer are in line with the experimental observations. Our calculated energetics suggests that the formation of *trans*-formato hydride is preferred over the *cis*-formato hydride species during the reaction, which is also corroborated with the experimental data, where the reactions between *cis*-[$Fe(dmpe)_2H_2$] and *cis*-[$Fe(PP_3)H_2$] (PP_3 = $P(CH_2CH_2PMe_2)_3$) with CO_2 results in the formation of stable *trans*-formato hydride *trans*-[$Fe(dmpe)_2(OCHO)H$].[53]

Based on the rate-limiting step and the catalyst regeneration steps identified with the Fe^{II} catalyst, we have demonstrated the role of Mn and Co ions in enhancing the reaction rate. If made, the Mn and Co catalysts will be better than the Fe catalyst with the reactivity following the order Co > Mn > Fe. From the sequence, it is clear that metal ions with open-shell electronic configurations as their ground state are more reactive than those with closed-shell ones, as shown by CASSCF calculations.

Various factors have been identified that play an important role in dictating the energy barrier for various transition states during the CO_2 hydrogenation reactions, for instance, destabilizing steric interaction and stabilizing orbital interaction energies. While all these factors are well established during the reaction catalyzed by both high-valent and low-valent metal catalysts, the effect of various open- and closed-shell electronic configurations in controlling the reactivity is unexplored. In the present study, we have looked into this aspect, where it is revealed that in a particular transition state, the total ground state wave function is composed of contributions from both open- and closed-shell configurations. Our results suggest that a larger contribution from the open-shell configurations at the transition state reduces the reaction barrier.

CONCLUSIONS

To this end, by employing an array of theoretical tools, we have established the origin of substrate-dependent product selectivity in the hydroboration of CO_2 using 3*d* metal ions. The ab initio CASSCF calculations on the transition states reveal strong configurational mixing of states that contribute to the substantial reduction of kinetic barriers in this challenging reaction. With the advent of AI/ML looking for various quantum descriptors to understand the reaction mechanism, the tool unveiled here has scope beyond the examples presented.

ASSOCIATED CONTENT

Supporting Information

The Supporting Information is available free of charge at https://pubs.acs.org/doi/10.1021/acs.inorgchem.2c02812.

Supporting figures; tables; and reaction coordinates (PDF)

AUTHOR INFORMATION

Corresponding Author

Gopalan Rajaraman − *Department of Chemistry, IIT Bombay, Powai 400076 Maharashtra, India;* orcid.org/0000-0001-6133-3026; Email: rajaraman@chem.iitb.ac.in

Authors

Asmita Sen − *Department of Chemistry, IIT Bombay, Powai 400076 Maharashtra, India*

Mursaleem Ansari − *Department of Chemistry, IIT Bombay, Powai 400076 Maharashtra, India*

Complete contact information is available at: https://pubs.acs.org/10.1021/acs.inorgchem.2c02812

Notes

The authors declare no competing financial interest.

ACKNOWLEDGMENTS

The authors thank SERB (CRG/2022/001697 and SB/SJF/2019-20/12) for funding. A.S. thanks CSIR for a fellowship. M.A. thanks IIT Bombay for an IPDF fellowship.

REFERENCES

(1) Dincer, I. Environmental impacts of energy. *Energy Policy* **1999**, *27*, 845−854.

(2) Dimitratos, N.; Lopez-Sanchez, J. A.; Hutchings, G. J. Green catalysis with alternative feedstocks. *Top. Catal.* **2009**, *52*, 258−268.
(3) Sakakura, T.; Choi, J.-C.; Yasuda, H. Transformation of carbon dioxide. *Chem. Rev.* **2007**, *107*, 2365−2387.
(4) Mikkelsen, M.; Jørgensen, M.; Krebs, F. C. The teraton challenge. A review of fixation and transformation of carbon dioxide. *Energy Environ. Sci.* **2010**, *3*, 43−81.
(5) Wang, W.-H.; Himeda, Y.; Muckerman, J. T.; Manbeck, G. F.; Fujita, E. CO2 hydrogenation to formate and methanol as an alternative to photo-and electrochemical CO2 reduction. *Chem. Rev.* **2015**, *115*, 12936−12973.
(6) Yu, K. M. K.; Curcic, I.; Gabriel, J.; Tsang, S. C. E. Recent advances in CO2 capture and utilization. *ChemSusChem* **2008**, *1*, 893−899.
(7) Jayarathne, U.; Hazari, N.; Bernskoetter, W. H. Selective iron-catalyzed N-formylation of amines using dihydrogen and carbon dioxide. *ACS Catal.* **2018**, *8*, 1338−1345.
(8) Ziebart, C.; Federsel, C.; Anbarasan, P.; Jackstell, R.; Baumann, W.; Spannenberg, A.; Beller, M. Well-defined iron catalyst for improved hydrogenation of carbon dioxide and bicarbonate. *J. Am. Chem. Soc.* **2012**, *134*, 20701−20704.
(9) Daw, P.; Chakraborty, S.; Leitus, G.; Diskin-Posner, Y.; Ben-David, Y.; Milstein, D. Selective N-formylation of amines with H2 and CO2 catalyzed by cobalt pincer complexes. *ACS Catal.* **2017**, *7*, 2500−2504.
(10) Mondal, B.; Song, J.; Neese, F.; Ye, S. Bio-inspired mechanistic insights into CO2 reduction. *Curr. Opin. Chem. Biol.* **2015**, *25*, 103−109.
(11) Fernández-Alvarez, F. J.; Aitani, A. M.; Oro, L. A. Homogeneous catalytic reduction of CO 2 with hydrosilanes. *Catal. Sci. Technol.* **2014**, *4*, 611−624.
(12) Jin, G.; Werncke, C. G.; Escudie, Y.; Sabo-Etienne, S.; Bontemps, S. Iron-catalyzed reduction of CO2 into methylene: Formation of C−N, C−O, and C−C bonds. *J. Am. Chem. Soc.* **2015**, *137*, 9563−9566.
(13) Kostera, S.; Peruzzini, M.; Gonsalvi, L. Recent Advances in Metal Catalyst Design for CO2 Hydroboration to C1 Derivatives. *Catalysts* **2021**, *11*, 58.
(14) Kinzel, N. W.; Werlé, C.; Leitner, W. Transition metal complexes as catalysts for the electroconversion of CO2: an organometallic perspective. *Angew. Chem., Int. Ed.* **2021**, *60*, 11628−11686.
(15) Obligacion, J. V.; Chirik, P. J. Earth-abundant transition metal catalysts for alkene hydrosilylation and hydroboration. *Nat. Rev. Chem.* **2018**, *2*, 15−34.
(16) Zhang, L.; Han, Z.; Zhao, X.; Wang, Z.; Ding, K. Highly efficient Ruthenium-catalyzed N-formylation of amines with H2 and CO2. *Angew. Chem.* **2015**, *127*, 6284−6287.
(17) Zhang, Y.; MacIntosh, A. D.; Wong, J. L.; Bielinski, E. A.; Williard, P. G.; Mercado, B. Q.; Hazari, N.; Bernskoetter, W. H. Iron catalyzed CO 2 hydrogenation to formate enhanced by Lewis acid co-catalysts. *Chem. Sci.* **2015**, *6*, 4291−4299.
(18) Federsel, C.; Ziebart, C.; Jackstell, R.; Baumann, W.; Beller, M. Catalytic hydrogenation of carbon dioxide and bicarbonates with a well-defined cobalt dihydrogen complex. *Chem. − Eur. J.* **2012**, *18*, 72−75.
(19) (a) Daw, P.; et al. Synthesis of Pyrazines and Quinoxalines via Acceptorless Dehydrogenative Coupling Routes Catalyzed by Manganese Pincer Complexes. *ACS Catal.* **2018**, *8*, 7734−7741. (b) Espinosa-Jalapa, N. A.; Kumar, A.; Leitus, G.; Diskin-Posner, Y.; Milstein, D. Synthesis of Cyclic Imides by Acceptorless Dehydrogenative Coupling of Diols and Amines Catalyzed by a Manganese Pincer Complex. *J. Am. Chem. Soc.* **2017**, *139*, 11722−11725.
(20) Bontemps, S.; Vendier, L.; Sabo-Etienne, S. Borane-Mediated Carbon Dioxide Reduction at Ruthenium: Formation of C1 and C2 Compounds. *Angew. Chem., Int. Ed.* **2012**, *51*, 1671−1674.
(21) Huang, F.; Zhang, C.; Jiang, J.; Wang, Z.-X.; Guan, H. How does the nickel pincer complex catalyze the conversion of CO2 to a methanol derivative? A computational mechanistic study. *Inorg. Chem.* **2011**, *50*, 3816−3825.
(22) Mondal, B.; Neese, F.; Ye, S. Toward rational design of 3d transition metal catalysts for CO2 hydrogenation based on insights into hydricity-controlled rate-determining steps. *Inorg. Chem.* **2016**, *55*, 5438−5444.
(23) Sokolovicz, Y. C. A.; Faza, O. N.; Specklin, D.; Jacques, B.; López, C. S.; dos Santos, J. H.; Schrekker, H. S.; Dagorne, S. Acetate-catalyzed hydroboration of CO 2 for the selective formation of methanol-equivalent products. *Catal. Sci. Technol.* **2020**, *10*, 2407−2414.
(24) Erken, C.; Kaithal, A.; Sen, S.; Weyhermüller, T.; Hölscher, M.; Werlé, C.; Leitner, W. Manganese-catalyzed hydroboration of carbon dioxide and other challenging carbonyl groups. *Nat. Commun.* **2018**, *9*, No. 4521.
(25) Espinosa, M. R.; Charboneau, D. J.; Garcia de Oliveira, A.; Hazari, N. Controlling Selectivity in the Hydroboration of Carbon Dioxide to the Formic Acid, Formaldehyde, and Methanol Oxidation Levels. *ACS Catal.* **2019**, *9*, 301−314.
(26) Jia, Z.; Li, L.; Zhang, X.; Yang, K.; Li, H.; Xie, Y.; Schaefer, H. F., III Acceleration Effect of Bases on Mn Pincer Complex-Catalyzed CO2 Hydroboration. *Inorg. Chem.* **2022**, *61*, 3970−3980.
(27) Zhang, L.; Zhao, Y.; Liu, C.; Pu, M.; Lei, M.; Cao, Z. Hydroboration of CO2 to Methyl Boronate Catalyzed by a Manganese Pincer Complex: Insights into the Reaction Mechanism and Ligand Effect. *Inorg. Chem.* **2022**, *61*, 5616−5625.
(28) Schaefer, B. A.; Margulieux, G. W.; Small, B. L.; Chirik, P. J. Evaluation of cobalt complexes bearing tridentate pincer ligands for catalytic C−H borylation. *Organometallics* **2015**, *34*, 1307−1320.
(29) Tamang, S. R.; Findlater, M. Emergence and applications of base metals (Fe, Co, and Ni) in hydroboration and hydrosilylation. *Molecules* **2019**, *24*, 3194.
(30) Roy, L.; Mondal, B.; Neese, F.; Ye, S.Theoretical Approach to Homogeneous Catalytic Reduction of CO_2: Mechanistic Understanding to Build New Catalysts. In *Carbon Dioxide Electrochemistry: Homogeneous and Heterogeneous Catalysis*; RSC Publications, 2020.
(31) Dong, C.; Ji, M.; Yang, X.; Yao, J.; Chen, H. Reaction mechanisms of CO2 reduction to formaldehyde catalyzed by hourglass Ru, Fe, and Os complexes: A density functional theory study. *Catalysts* **2017**, *7*, 5.
(32) Frisch, M.; Trucks, G.; Schlegel, H.; Scuseria, G.; Robb, M.; Cheeseman, J.; Scalmani, G.; Barone, V.; Petersson, G.; Nakatsuji, H. *Gaussian 16*, revision C.01; Gaussian Inc.: Wallingford, CT, 2016.
(33) Zhao, Y.; Truhlar, D. G. A new local density functional for main-group thermochemistry, transition metal bonding, thermochemical kinetics, and non-covalent interactions. *J. Chem. Phys.* **2006**, *125*, No. 194101.
(34) Hay, P. J.; Wadt, W. R. Ab initio effective core potentials for molecular calculations. Potentials for the transition metal atoms Sc to Hg. *J. Chem. Phys.* **1985**, *82*, 270−283.
(35) Verma, P.; Varga, Z.; Klein, J. E.; Cramer, C. J.; Que, L.; Truhlar, D. G. Assessment of electronic structure methods for the determination of the ground spin states of Fe (II), Fe (III) and Fe (IV) complexes. *Phys. Chem. Chem. Phys.* **2017**, *19*, 13049−13069.
(36) Mondal, B.; Neese, F.; Ye, S. Control in the rate-determining step provides a promising strategy to develop new catalysts for CO2 hydrogenation: a local pair natural orbital coupled cluster theory study. *Inorg. Chem.* **2015**, *54*, 7192−7198.
(37) Zheng, J.; Xu, X.; Truhlar, D. G. Minimally augmented Karlsruhe basis sets. *Theor. Chem. Acc.* **2011**, *128*, 295−305.
(38) Marenich, A. V.; Cramer, C. J.; Truhlar, D. G. Universal solvation model based on solute electron density and on a continuum model of the solvent defined by the bulk dielectric constant and atomic surface tensions. *J. Phys. Chem. B* **2009**, *113*, 6378−6396.
(39) Neese, F.; Wennmohs, F.; Becker, U.; Riplinger, C. The ORCA quantum chemistry program package. *J. Chem. Phys.* **2020**, *152*, No. 224108.

https://doi.org/10.1021/acs.inorgchem.2c02812
Inorg. Chem. 2023, 62, 3727−3737

(40) Reiher, M. Douglas−Kroll−Hess Theory: a relativistic electrons-only theory for chemistry. *Theor. Chem. Acc.* **2006**, *116*, 241−252.
(41) Roos, B. O.The Complete Active Space Self-Consistent Field Method and Its Applications in Electronic Structure Calculations. In *Advances in Chemical Physics*; Wiley, 1987; Vol. *69*, pp 399−445.
(42) Roy, L.; Al-Afyouni, M. H.; DeRosha, D. E.; Mondal, B.; DiMucci, I. M.; Lancaster, K. M.; Shearer, J.; Bill, E.; Brennessel, W. W.; Neese, F.; et al. Reduction of CO2 by a masked two-coordinate cobalt (i) complex and characterization of a proposed oxodicobalt (ii) intermediate. *Chem. Sci.* **2019**, *10*, 918−929.
(43) Leto, D. F.; Massie, A. A.; Rice, D. B.; Jackson, T. A. Spectroscopic and computational investigations of a mononuclear manganese (IV)-oxo complex reveal electronic structure contributions to reactivity. *J. Am. Chem. Soc.* **2016**, *138*, 15413−15424.
(44) Rice, D. B.; Massie, A. A.; Jackson, T. A. Experimental and Multireference ab Initio Investigations of Hydrogen-Atom-Transfer Reactivity of a Mononuclear MnIV-oxo Complex. *Inorg. Chem.* **2019**, *58*, 13902−13916.
(45) Cho, K.-B.; Shaik, S.; Nam, W. Theoretical investigations into C−H Bond activation reaction by nonheme MnIVO complexes: multistate reactivity with no oxygen rebound. *J. Phys. Chem. Lett.* **2012**, *3*, 2851−2856.
(46) Sen, A.; Rajaraman, G. Does the Spin State and Oriented External Electric Field Boost the Efficiency of Fe(II) Pincer Catalyst toward CO_2 Hydrogenation Reaction? *Inorg. Chem.* **2023**, *62* (5), 2342.
(47) Ahlquist, M. S. Iridium catalyzed hydrogenation of CO2 under basic conditions—Mechanistic insight from theory. *J. Mol. Catal. A* **2010**, *324*, 3−8.
(48) (a) Yang, X. Hydrogenation of Carbon Dioxide Catalyzed by PNP Pincer Iridium, Iron, and Cobalt Complexes: A Computational Design of Base Metal Catalysts *ACS Catal. 1* 849 854 DOI: 10.1021/cs2000329. (b) Yang, X. Unexpected Direct Reduction Mechanism for Hydrogenation of Ketones Catalyzed by Iron PNP Pincer Complexes. *Inorg. Chem.* **2011**, *50*, 12836−12843.
(49) Ogo, S.; Kabe, R.; Hayashi, H.; Harada, R.; Fukuzumi, S. Mechanistic investigation of CO 2 hydrogenation by Ru (II) and Ir (III) aqua complexes under acidic conditions: two catalytic systems differing in the nature of the rate determining step. *Dalton Trans.* **2006**, *39*, 4657−4663.
(50) Whittlesey, M. K.; Mawby, R. J.; Osman, R.; Perutz, R. N.; Field, L. D.; Wilkinson, M. P.; George, M. W. Transient and matrix photochemistry of Fe (dmpe) 2H2 (dmpe = Me2PCH2CH2Me2): dynamics of CH and HH activation. *J. Am. Chem. Soc.* **1993**, *115*, 8627−8637.
(51) Allen, O. R.; Dalgarno, S. J.; Field, L. D. Reductive disproportionation of carbon dioxide at an Iron (II) center. *Organometallics* **2008**, *27*, 3328−3330.
(52) Dai, H.; Guan, H. Iron dihydride complexes: synthesis, reactivity, and catalytic applications. *Isr. J. Chem.* **2017**, *57*, 1170−1203.
(53) Field, L. D.; Lawrenz, E. T.; Shaw, W. J.; Turner, P. Insertion of CO2, CS2, and COS into Iron (II)− Hydride bonds. *Inorg. Chem.* **2000**, *39*, 5632−5638.

https://doi.org/10.1021/acs.inorgchem.2c02812
Inorg. Chem. 2023, 62, 3727−3737